ACS APPLIED MATERIALS & INTERFACES

Letter

www.acsami.org

Free-Floating Synthetic Nanosheets by Atomic Layer Deposition

Kyoungmi Lee, Do Han Kim, and Gregory N. Parsons*

Department of Chemical and Biomolecular Engineering, North Carolina State University, Raleigh, North Carolina 27695, United States

Supporting Information

ABSTRACT: Two-dimensional (2D) nanosheets with distinctive properties are often fabricated by exfoliation, hydrothermal synthesis, or vapor-phase reaction. While these approaches are useful to generate nanosheets, we show that free-floating 2D metal oxide flakes with nanometer-scale thickness can also be formed by atomic layer deposition (ALD), where the ALD process allows the thickness and composition to be precisely tuned. In this work, we describe in detail the ALD nanosheet fabrication process and demonstrate how the choice of the sacrificial substrate affects the subsequent ALD processing and the resulting nanosheet thickness and surface structure. In addition, we introduce the fabrication of organic/inorganic bilayer nanosheets with unique potential applications.

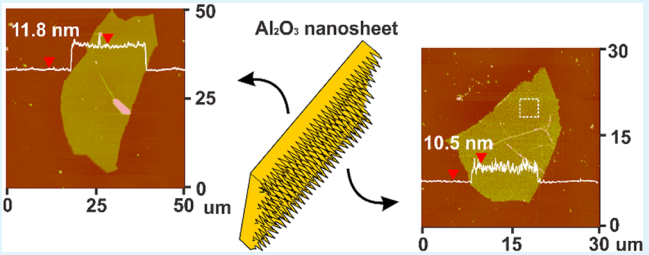

KEYWORDS: *nanosheet, atomic layer deposition, sacrificial polymer, organic/inorganic sheet*

Recently, many types of two-dimensional (2D) nanosheet materials are being developed and modified for applications in nanoelectronics,[1] biomedicine,[2] energy-storage devices,[3] or biomaterial systems.[4] Since graphene was first isolated from graphite in 2004,[5] a vast amount of research has revealed its unusual electronic and physical properties such as high electron mobility and quantum Hall effect.[6] While graphene has a potential application as a conductor, various oxides[7] including perovskite that have naturally stacked molecular structures also show semiconducting or high κ-dielectric properties.[8]

Table 1 summarizes the fabrication methods and thickness range for several nanosheet materials studied to date. The two primary methods for nanosheet fabrication are hydrothermal synthesis and exfoliation from layered compounds.[9−18] Because exfoliation is applied for compounds with naturally stacked molecular structure, it normally produces thinner nanosheets than other methods. Other functional materials, such as silver, gold, or platinum nanoparticles, are often added to nanosheets to enhance the performance in biosensors, batteries, or solar-cell structures.[19−21] Recent work shows that WO_3 formed by atomic layer deposition (ALD) can be converted to WS_2 nanosheets by reaction with H_2S at 1000 °C, and they show good performance in field-effect-transistor structures.[22] The unique functionality of 2D nanosheets is determined to a large extent by the electronic structure associated with full crystallinity, well-defined electronic surface termination and occupation, as well as the planar morphology and high surface area. For example, the electronic structure of 2D graphene rapidly changes with increasing layers, reaching its full three-dimensional limit at ∼10 graphene multilayers,[6] a few nanometers thick. Previously, we showed that ALD can be used to fabricate free-floating metal oxide nanosheets at low temperatures with thickness in the range of 2D electronic materials.[23] While the ALD materials formed at low temperature do not have full crystalline morphology and well-defined regular surface structure of graphene or other 2D solids, the

Table 1. Fabrication Methods and Thicknesses of Nanosheets

methods		materials	thickness (nm)	ref
exfoliation		graphene	<1	9
		MoS_2	<1	10
		MnO_2	<1	11
		BN	1−7	12
	perovskite	$Ca_2Nb_3O_{10}$	∼1	13
		$K_2Ln_2Ti_3O_{10}$, $KLnNb_2O_7$, $RbLnTa_2O_7$	1−3	14
hydrothermal synthesis		NiO	30−50	15
		ZnO	50	16
		TiO_2	10−15	17
		$BiVO_4$	10−40	18
thermal evaporation		Ga_2O_3	20−60	24
		ZnS	tens of nanometers	25
ALD + postdeposition reaction		WS_2	1−30	22
ALD		Al_2O_3, ZnO, TiO_2	1−17	23

Received: May 8, 2014
Accepted: June 30, 2014
Published: June 30, 2014

ALD process provides several unique advantages for 2D structure synthesis. Specifically, ALD allows (1) access to a wide material set, beyond known 2D crystal materials, (2) direct scalability to large areas with well-controlled thickness, and (3) facile fabrication of multicomponent heterojunctions and other multiple-compound-layered structures. For example, a TiO_2/ZnO ALD bilayer nanosheet deposited at 100 and 90 °C has photocatalytic functionality, and the rates of photocatalytic decomposition followed the expected trends in light intensity and thickness. More importantly, bilayer nanosheets composed of TiO_2/ZnO (2.5 nm/2.5 nm) also deposited at 100 and 90 °C improve the dye degradation rate by ~5 times over TiO_2 nanosheets (2.5 nm). The previous work did not show a detailed analysis of the ALD film nucleation and how it is affected by precursor and substrate choices. This information will be important to further tune and optimize 2D ALD material fabrication.

Here, we report in detail the effects of polymers used as a sacrificial layer and ALD materials on nanosheet synthesis. Specific sacrificial polymer substrates include poly(methyl methacrylate) (PMMA), poly(vinyl alcohol) (PVA), and poly(acrylic acid) (PAA). We observed that PVA is most suitable to separate the ALD film with larger size among the tested polymers. From PVA sacrificial layers, the thicknesses of the resulting nanosheets, as observed by ellipsometry and atomic force microscopy (AFM), match precisely the thickness of ALD films formed simultaneously on planar silicon substrates. In addition, we demonstrate the feasibility of using selective polymer dissolution to create free-floating organic/inorganic bilayer sheets, where one nanosheet face is organic and the other inorganic.

Many polymers are known to react with metal−organic precursors during ALD to produce subsurface growth and a graded organic/inorganic interface layer.[26−28] Some polymers, however, including PVA and PAA, have hydroxyl groups present on the surface that can provide good nucleation sites for metal oxide ALD,[27] helping to promote surface nucleation and form an abrupt organic/inorganic interface.[26,28] Carbonyl groups (C═O) in PMMA also react with a precursor to initiate nucleation.[29] In the case of PMMA, however, precursors can diffuse more through the polymer layers than PVA and PAA.

To fabricate nanosheets, sacrificial polymers were spun-cast onto oxidized silicon followed by ALD in a custom hot-wall viscous flow tube reactor. After ALD, the film was cut with a razor blade before polymer dissolution in a liquid solvent. For imaging, nanosheets were collected on clean oxidized silicon and annealed in air to remove residual polymer.

Several experiments tested PMMA as a sacrificial layer for Al_2O_3 nanosheet formation. We found, for example, that when spun-cast PMMA was exposed to 100 cycles of tetramethylammonium (TMA)/water at 90 °C, the subsequent polymer dissolution step in toluene caused the ALD overlayers to rip or tear, especially for the thinner films. However, when PAA was used as a sacrificial layer, its high solubility and low molecular weight (MW) led to very fast dissolution in water.[30] The rapid dissolution likely added stress to the adhered ALD layer, causing the thin layer to break and fracture into small pieces less than 1 μm across. The PVA polymer also showed good solubility in water, but it dissolved more slowly, allowing the coated film to flow off more gently, thereby maintaining larger sheets, up to 5 mm across, that were more easily collected and analyzed. If the substrate dissolves too slowly, however, it is difficult to determine the stopping point for complete organic removal. For the PVA materials, we tested materials with high and low MW, 95000 and 16000 g/mol, respectively. The faster-dissolving low-MW PVA tended to show the best dissolution properties, where the speed was high enough to ensure complete organic removal but slow enough to maintain the coating physical structure. Unless otherwise specified, the nanosheet materials described here were fabricated using the low-MW PVA.

Figure 1 shows optical microscopic images of Al_2O_3, TiO_2, and ZnO ALD nanosheets with various film thicknesses. Each

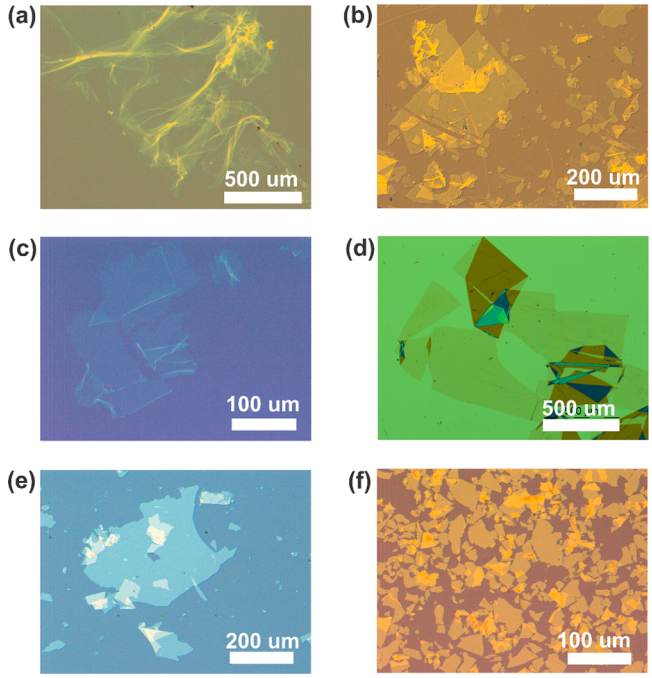

Figure 1. Optical microscopic images of Al_2O_3 nanosheets exfoliated from low-MW PVA substrates after (a) 10 and (b) 50 cycles. Also shown are TiO_2 nanosheets formed using (c) 25 and (d) 300 cycles, as well as ZnO nanosheets from (e) 100 and (f) 150 cycles.

type of nanosheet shows properties characteristic of the material. For example, in Figure 1a, the Al_2O_3 nanosheets made using 10 ALD cycles show a folded structure with rounded edges, indicating high flexibility. The wrinkling and overlap evident in the thin ~1.1 nm nanosheets is less evident in the ~5-nm-thick sheets shown in Figure 1b. The thicker films also show a sharper edge shape. Similar to the thin Al_2O_3, the edges of thin ~1.3 nm TiO_2 nanosheets shown in Figure 1c are curved and rolled up, while the 15.5-nm-thick TiO_2 nanosheets in Figure 1d have angular shape. Also, the thicker ZnO nanosheets tend to break into smaller pieces (Figure 1f), suggesting that thinner sheets are more flexible. The different contrast or color in different regions in Figure 1d is resulted from optical interference due to the stacking or overlap of nanosheets at various points on the surface.

We worked to determine the lower thickness limit for reliable nanosheet fabrication for the materials studied. For Al_2O_3 and TiO_2, the thinnest sheets we could consistently isolate and optically image were 1.1 and 1.3 nm, as shown in Figure 1a,c. We were also able to isolate Al_2O_3 nanosheets after 5 ALD cycles. These were 0.8 nm thick, as determined by AFM, but we could not obtain a clear optical image. We found it difficult to achieve large-area ZnO nanosheets of less than ~17 nm thick.

Figure 1e shows ZnO nanosheets formed from 100 ALD cycles, corresponding to 17.2 nm. This was close the lower limit of the ZnO layer thickness that we could separate as a stable cohesive nanosheet film. Somewhat thicker ZnO nanosheets are shown in Figure 1f.

When ZnO was deposited on the polymer using less than 100 cycles, dissolving the polymer led to film separation into small flat particles. These particles were small ZnO crystal grains or crystal grain clusters that were not connected into a cohesive film. Figure 2a shows the TEM image of ZnO

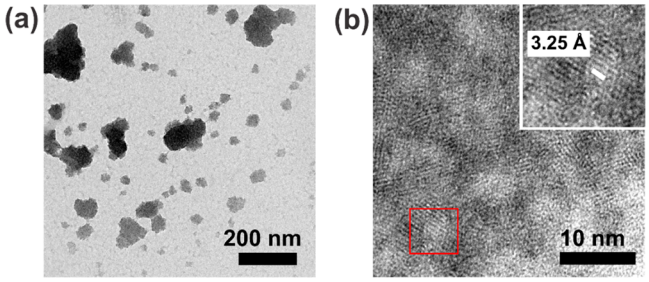

Figure 2. TEM images of ZnO nanosheets from 50 ALD cycles: (a) ZnO nanosheets showing a size of less than 200 nm; (b) lattice spacing of 3.25 Å confirming ZnO crystallinity.

nanosheets from 50 ALD cycles. They mostly show a lateral dimension of less than ~200 nm. Despite of the smaller size, the crystallinity of ZnO is confirmed by TEM images shown in Figure 2b, which shows α lattice spacing of wurtzite ZnO.[31]

When the nanosheets were formed on the polymer, films were simultaneously deposited onto a clean oxidized silicon wafer, and these monitor wafers were used to measure the film thickness using ellipsometry. The nanosheet thickness was also analyzed by AFM, where the nanosheets were removed from the polymer and transferred to flat silicon wafers as discussed above. Figure 3 shows the layer thickness obtained by ellipsometry and AFM plotted against the number of ALD cycles for Al_2O_3, ZnO, and TiO_2 nanosheets. In all cases, the nanosheet thickness corresponds well to the thickness of the film directly deposited on silicon, with nanosheet thickness down to the ~1 nm range. This correlation held true even for the small ZnO particles formed with 50 ALD cycles (Figure

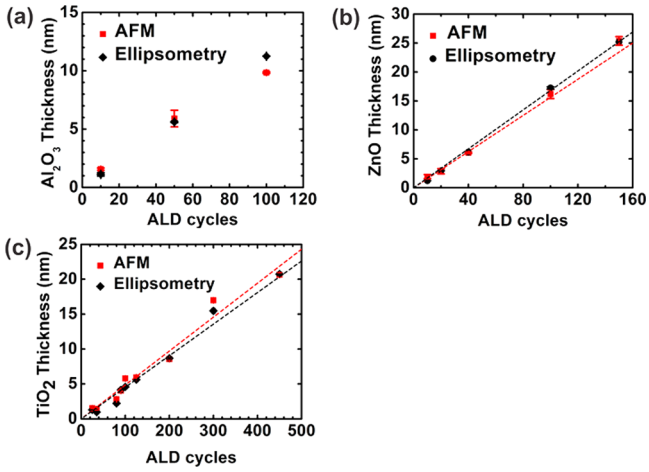

Figure 3. Graphs comparing the nanosheet thickness measured from AFM to the film thickness from ellipsometry depending on the ALD cycles for (a) Al_2O_3, (b) ZnO, and (c) TiO_2.

3b). These graphs indicate that ALD is an effective way to attain a range of metal oxides in the nanosheet format, where the thickness can be readily tuned by the number of ALD cycles used.

The surface roughness of the resulting nanosheets is also of interest. Figure 4a shows an AFM image of the Al_2O_3

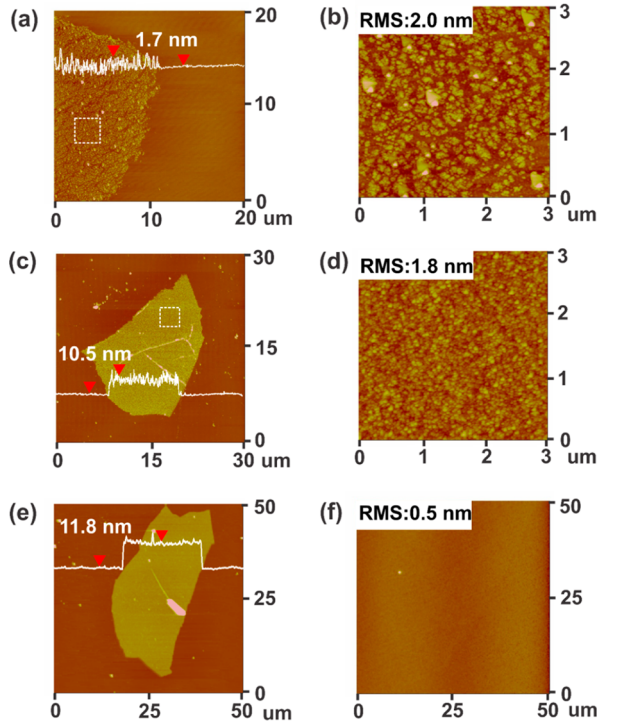

Figure 4. AFM image of the Al_2O_3 nanosheet obtained from (a) 5 and (c) 100 ALD cycles. (b and d) Magnified images inside the nanosheet marked with the dotted box from parts a and b. (e) Al_2O_3 nanosheet from 100 ALD cycles with a smooth surface. (f) AFM image of spin-coated PVA (MW = 16000 g/mol) used as a sacrificial layer.

nanosheet obtained after 5 ALD cycles. Figure 4b displays a more magnified image collected from the 3 μm box region in Figure 4a, showing a root-mean-square (rms) roughness of ~2.0 nm. This thin nanosheet is a single continuous 2D film with rough surface texture, and the contrast in the AFM image makes it appear as a composite of many individual flakes. During the Al_2O_3 nucleation phase, i.e., the first 10–20 ALD cycles, small Al_2O_3 clusters coalesce to form a continuous film,[26,28] so the surface roughness in the ~5 nm nanosheets likely relates to film nucleation on the polymer substrate. Parts c and d of Figure 4 show similar AFM images at the same scale obtained from a 10.5-nm-thick Al_2O_3 nanosheet formed using 100 ALD cycles. This layer shows an rms of 1.8 nm, nearly the same as the 5-cycle sample. However, Figure 4e shows a different nanosheet formed in the same run as the one in Figure 4c,d. This second nanosheet shows a remarkably smoother surface, with a rms roughness of ~1.1 nm. This difference in the nanosheet roughness is attributed to different roughness on the "front" and "back" of the nanosheets. Surveying a random set of the thicker nanosheets collected from a single batch shows a roughly binary distribution of surface roughness, with half showing relatively rough surface texture and half showing smoother texture. We ascribe the rougher texture to the "bottom" of the nanosheet, which is the side originally in contact with the polymer substrate, and the smoother texture to

the "top" of the nanosheet on the deposited film face. To help confirm this assignment, Figure 4f shows an AFM image of the sacrificial PVA layer after spin coating before the ALD nanosheet coating step. The PVA layer shows an rms roughness of 0.5 nm. Even though PVA has surface hydroxyl groups that can readily react with TMA, some subsurface diffusion may occur, leading to roughness on the "bottom" of the nanosheet that exceeds the roughness of the starting substrate. The difference in surface roughness from bottom to top in the thicker nanosheets suggests that the roughness evolves from surface processes during film growth rather than conformal transfer of substrate texture to the deposited coating. Variation in the nanosheet thickness after 100 ALD cycles in Figure 4c,e is attributed to differences in the residual polymer remaining after annealing at 450−500 °C for 1 h.

We note that some of the nanosheets retain large lateral size (Figure 1a−e), while the thicker ZnO layers tend to break upon polymer dissolution (Figures 1f and 2). The more amorphous Al_2O_3 and TiO_2 nanosheets appear to be more flexible, allowing larger sizes to be attained.

We also explored the creation of organic/inorganic bilayer heterojunction sheets. These layers were also formed on a thin (<1000 nm) sacrificial PAA or PVA layer formed from an aqueous solution. A second polymer, in this case PMMA dissolved in tetrahydrofuran, was spun coat onto PAA or PVA. Because PMMA dissolves in different solvents from PAA or PVA, they are expected to be immiscible. The resulting polymer stack is then exposed to 100 ALD cycles of TiO_2 at 100 °C or 100 ALD cycles of ZnO at 90 °C. Dissolving PAA or PVA then results in a free-floating organic/inorganic bilayer sheet stack or junction. Parts a and b of Figure 5 show digital photographs of

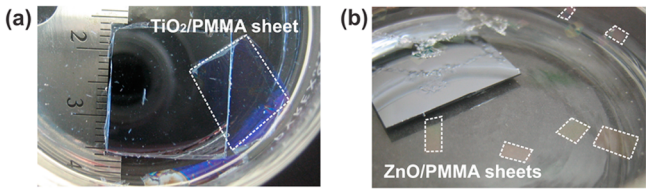

Figure 5. Pictures of (a) TiO_2/PMMA bilayer sheets separated during PAA dissolution and (b) ZnO/PMMA bilayer sheets during PVA dissolution.

TiO_2/PMMA and ZnO/PMMA bilayer sheets separated from the substrate after dissolution of PAA or PVA. For the TiO_2/PMMA bilayer sheet, the substrate was scribed once using a razor blade before PAA dissolution, resulting in large nanosheets, ∼1 cm across (Figure 5a). For the ZnO/PMMA bilayer sheets, several razor scribes were cut into the coated sample, resulting in a larger number of smaller nanosheets, a few millimeters across (Figure 5b).

Several researchers study inorganic materials coordinated with organics for a variety of applications. For example, Stroock et al.[32] demonstrated free-floating polymer flakes with well-defined size and shape using microcontact printing and selective surface polymerization. Also, Vendamme et al.[33] showed free-standing ∼35-nm-thick organic/inorganic interpenetrating network membranes formed by liquid-phase sol−gel methods. The ALD organic/inorganic bilayers are unique in that they have separate organic and inorganic regions, opposite-facing on different sides of the heterogeneous nanosheet. Such hybrid materials may find unique uses in the fields of electronics, optics, or bioengineering.[34]

This work demonstrates ALD as a viable means to prepare free-floating nanosheet materials. The results describe the role of the sacrificial polymers and ALD process on the resulting structures. We find that PVA with MW = 16000 g/mol performed well as a sacrificial substrate, allowing the formation of synthetic Al_2O_3, ZnO, and TiO_2 nanosheets with thickness down to 1 nm and a lateral size-to-thickness ratio exceeding 20000. The nanosheet thickness measured by AFM correlates directly with the thickness of films formed simultaneously on planar solid surfaces. The surface roughness of the resulting nanosheets reflects processes that occur during film nucleation and growth rather than transferring the substrate roughness through conformal film evolution. For some processes, a binary distribution of surface roughness values is obtained, likely because of different roughness on the "front" and "back" of the nanosheets. ZnO nanosheets consisting of dispersed crystal grains or clusters with smaller lateral dimension were obtained using 50 ZnO ALD cycles on PVA. Moreover, the ALD process allows the facile fabrication of multilayered nanosheet structures, including inorganic/inorganic and organic/inorganic bilayers.

■ ASSOCIATED CONTENT

Ⓢ Supporting Information

Experimental details. This material is available free of charge via the Internet at http://pubs.acs.org.

■ AUTHOR INFORMATION

Corresponding Author

*E-mail: parsons@ncsu.edu.

Notes

The authors declare no competing financial interest.

■ ACKNOWLEDGMENTS

This work was supported by the National Science Foundation under Grant CBET-1034374.

■ REFERENCES

(1) Osada, M.; Sasaki, T. 2D Oxide Nanosheets: Controlled Assembly and Applications. *ECS Trans.* **2013**, *50*, 111−116.

(2) Ventrelli, L.; Ricotti, L.; Menciassi, A.; Mazzolai, B.; Mattoli, V. Nanoscaffolds for Guided Cardiac Repair: The New Therapeutic Challenge of Regenerative Medicine. *J. Nanomater.* **2013**, *2013*, 1−16.

(3) Mhamane, D.; Suryawanshi, A.; Banerjee, A.; Aravindan, V.; Ogale, S.; Srinivasan, M. Non-Aqueous Energy Storage Devices Using Graphene Nanosheets Synthesized by Green Route. *AIP Adv.* **2013**, *3*, 042112.

(4) Nabetani, Y.; Takamura, H.; Hayasaka, Y.; Sasamoto, S.; Tanamura, Y.; Shimada, T.; Masui, D.; Takagi, S.; Tachibana, H.; Tong, Z.; et al. An Artificial Muscle Model Unit Based on Inorganic Nanosheet Sliding by Photochemical Reaction. *Nanoscale* **2013**, *5*, 3182−3193.

(5) Novoselov, K. S.; Geim, A. K.; Morozov, S. V.; Jiang, D.; Zhang, Y.; Dubonos, S. V.; Grigorieva, I. V.; Firsov, A. A. Electric Field Effect in Atomically Thin Carbon Films. *Science* **2004**, *306*, 666−669.

(6) Geim, A. K.; Novoselov, K. S. The rise of graphene. *Nat. Mater.* **2007**, *6*, 183−191.

(7) Ma, R. Z.; Sasaki, T. Nanosheets of Oxides and Hydroxides: Ultimate 2D Charge-Bearing Functional Crystallites. *Adv. Mater.* **2010**, *22*, 5082−5104.

(8) Osada, M.; Ebina, Y.; Funakubo, H.; Yokoyama, S.; Kiguchi, T.; Takada, K.; Sasaki, T. High-κ Dielectric Nanofilms Fabricated from Titania Nanosheets. *Adv. Mater.* **2006**, *18*, 1023−1027.

(9) Guo, H.-L.; Wang, X.-F.; Qian, Q.-Y.; Wang, F.-B.; Xia, X.-H. A Green Approach to the Synthesis of Graphene Nanosheets. *ACS Nano* **2009**, *3*, 2653−2659.
(10) Radisavljevic, B.; Radenovic, A.; Brivio, J.; Giacometti, V.; Kis, A. Single-Layer MoS_2 Transistors. *Nat. Nanotechnol.* **2011**, *6*, 147−150.
(11) Wang, L.; Omomo, Y.; Sakai, N.; Fukuda, K.; Nakai, I.; Ebina, Y.; Takada, K.; Watanabe, M.; Sasaki, T. Fabrication and Characterization of Multilayer Ultrathin Films of Exfoliated MnO_2 Nanosheets and Polycations. *Chem. Mater.* **2003**, *15*, 2873−2878.
(12) Lin, Y.; Williams, T. V.; Connell, J. W. Soluble, Exfoliated Hexagonal Boron Nitride Nanosheets. *J. Phys. Chem. Lett.* **2010**, *1*, 277−283.
(13) Ebina, Y.; Sasaki, T.; Harada, M.; Watanabe, M. Restacked Perovskite Nanosheets and Their Pt-Loaded Materials as Photocatalysts. *Chem. Mater.* **2002**, *14*, 4390−4395.
(14) Ida, S.; Ogata, C.; Eguchi, M.; Youngblood, W. J.; Mallouk, T. E.; Matsumoto, Y. Photoluminescence of Perovskite Nanosheets Prepared by Exfoliation of Layered Oxides, $K_2Ln_2Ti_3O_{10}$, $KLnNb_2O_7$, and $RbLnTa_2O_7$ (Ln: lanthanide ion). *J. Am. Chem. Soc.* **2008**, *130*, 7052−7059.
(15) Zou, Y.; Wang, Y. NiO Nanosheets Grown on Graphene Nanosheets as Superior Anode Materials for Li-Ion Batteries. *Nanoscale* **2011**, *3*, 2615−2620.
(16) Wang, Y.; Fan, X.; Sun, J. Hydrothermal Synthesis of Phosphate-Mediated ZnO Nanosheets. *Mater. Lett.* **2009**, *63*, 350−352.
(17) Yu, J.; Fan, J.; Lv, K. Anatase TiO_2 Nanosheets with Exposed (001) Facets: Improved Photoelectric Conversion Efficiency in Dye-Sensitized Solar Cells. *Nanoscale* **2010**, *2*, 2144−2149.
(18) Zhang, L.; Chen, D.; Jiao, X. Monoclinic Structured $BiVO_4$ Nanosheets: Hydrothermal Preparation, Formation Mechanism, and Coloristic and Photocatalytic Properties. *J. Phys. Chem. B* **2006**, *110*, 2668−2673.
(19) Liu, J.; Fu, S.; Yuan, B.; Li, Y.; Deng, Z. Toward a Universal "Adhesive Nanosheet" for the Assembly of Multiple Nanoparticles Based on a Protein-Induced Reduction/Decoration of Graphene Oxide. *J. Am. Chem. Soc.* **2010**, *132*, 7279−7281.
(20) Guo, S.; Wen, D.; Zhai, Y.; Dong, S.; Wang, E. Platinum Nanoparticle Ensemble-on-Graphene Hybrid Nanosheet: One-Pot, Rapid Synthesis, and Used as New Electrode Material for Electrochemical Sensing. *ACS Nano* **2010**, *4*, 3959−3968.
(21) Liang, J.; Chen, Z.; Guo, L.; Li, L. Electrochemical Sensing of l-Histidine Based on Structure-Switching DNAzymes and Gold Nanoparticle−Graphene Nanosheet Composites. *Chem. Commun.* **2011**, *47*, 5476−5478.
(22) Song, J.-G.; Park, J.; Lee, W.; Choi, T.; Jung, H.; Lee, C. W.; Hwang, S.-H.; Myoung, J. M.; Jung, J.-H.; Kim, S.-H. Layer-Controlled, Wafer-Scale, and Conformal Synthesis of Tungsten Disulfide Nanosheets Using Atomic Layer Deposition. *ACS Nano* **2013**, *7*, 11333−11340.
(23) Lee, K.; Losego, M. D.; Kim, D. H.; Parsons, G. N. High Performance Photocatalytic Metal Oxide Synthetic Bi-Component Nanosheets Formed by Atomic Layer Deposition. *Mater. Horiz.* **2014**, *1*, 419−423.
(24) Dai, Z. R.; Pan, Z. W.; Wang, Z. L. Gallium Oxide Nanoribbons and Nanosheets. *J. Phys. Chem. B* **2002**, *106*, 902−904.
(25) Liang, C.; Shimizu, Y.; Sasaki, T.; Umehara, H.; Koshizaki, N. Au-Mediated Growth of Wurtzite ZnS Nanobelts, Nanosheets, and Nanorods via Thermal Evaporation. *J. Phys. Chem. B* **2004**, *108*, 9728−9733.
(26) Wilson, C. A.; Grubbs, R. K.; George, S. M. Nucleation and Growth during Al_2O_3 Atomic Layer Deposition on Polymers. *Chem. Mater.* **2005**, *17*, 5625−5634.
(27) Hyde, G. K.; Scarel, G.; Spagnola, J. C.; Peng, Q.; Lee, K.; Gong, B.; Roberts, K. G.; Roth, K. M.; Hanson, C. A.; Devine, C. K.; et al. Atomic Layer Deposition and Abrupt Wetting Transitions on Nonwoven Polypropylene and Woven Cotton Fabrics. *Langmuir* **2010**, *26*, 2550−2558.
(28) Jur, J. S.; Spagnola, J. C.; Lee, K.; Gong, B.; Peng, Q.; Parsons, G. N. Temperature-Dependent Subsurface Growth during Atomic Layer Deposition on Polypropylene and Cellulose Fibers. *Langmuir* **2010**, *26*, 8239−8244.
(29) Peng, Q.; Tseng, Y. C.; Darling, S. B.; Elam, J. W. Nanoscopic Patterned Materials with Tunable Dimensions via Atomic Layer Deposition on Block Copolymers. *Abs. Pap. Am. Chem. Soc.* **2010**, *240*.
(30) Linder, V.; Gates, B. D.; Ryan, D.; Parviz, B. A.; Whitesides, G. M. Water-Soluble Sacrificial Layers for Surface Micromachining. *Small* **2005**, *1*, 730−736.
(31) Pan, Z. W.; Dai, Z. R.; Wang, Z. L. Nanobelts of Semiconducting Oxides. *Science* **2001**, *291*, 1947−1949.
(32) Stroock, A. D.; Kane, R. S.; Weck, M.; Metallo, S. J.; Whitesides, G. M. Synthesis of Free-Standing Quasi-Two-Dimensional Polymers. *Langmuir* **2003**, *19*, 2466−2472.
(33) Vendamme, R.; Onoue, S.-Y.; Nakao, A.; Kunitake, T. Robust Free-Standing Nanomembranes of Organic/Inorganic Interpenetrating Networks. *Nat. Mater.* **2006**, *5*, 494−501.
(34) Kagan, C. R.; Mitzi, D. B.; Dimitrakopoulos, C. D. Organic−Inorganic Hybrid Materials as Semiconducting Channels in Thin-Film Field-Effect Transistors. *Science* **1999**, *286*, 945−947.